Vibrational dynamics of confined granular materials

Emilien Azéma,* Farhang Radjaï, Robert Peyroux, and Frédéric Dubois
LMGC, CNRS - Université Montpellier II, Place Eugène Bataillon, 34095 Montpellier Cedex 05, France

Gilles Saussine
Physics of Railway Systems, Innovation and Research Department of SNCF, 45 rue de Londres, 75379 Paris Cedex 08, France
(Received 22 April 2006; published 13 September 2006)

By means of two-dimensional contact dynamics simulations, we analyze the vibrational dynamics of a confined granular layer in response to harmonic forcing. We use irregular polygonal grains allowing for strong variability of solid fraction. The system involves a jammed state separating passive (loading) and active (unloading) states. We show that an approximate expression of the packing resistance force as a function of the displacement of the free retaining wall from the jamming position provides a good description of the dynamics. We study in detail the scaling of displacements and velocities with loading parameters. In particular, we find that, for a wide range of frequencies, the data collapse by scaling the displacements with the inverse square of frequency, the inverse of the force amplitude, and the square of gravity. Interestingly, compaction occurs during the extension of the packing, followed by decompaction in the contraction phase. We show that the mean compaction rate increases linearly with frequency up to a characteristic frequency and then it declines in inverse proportion to frequency. The characteristic frequency is interpreted in terms of the time required for the relaxation of the packing through collective grain rearrangements between two equilibrium states.

DOI: 10.1103/PhysRevE.74.031302 PACS number(s): 83.80.Fg, 61.43.Gt

I. INTRODUCTION

Depending on the frequency and amplitude of accelerations, vibrated granular materials give rise to various phenomena such as compaction [1,2], convective flow [3–5], size segregation, and standing-wave patterns at the free surface [3,6,7]. Particle rearrangements induced by vibrations lead to lower shear strength and larger flowability. In the full fluidization regime, there are no permanent contacts between particles and the system behaves as a dissipative gas [8]. Particle-bed reactors are sometimes fluidized by this method instead of upward gas flow [9]. When particle accelerations remain below the gravitational acceleration, the system keeps its static nature and the vibrational energy propagates through a rather compact network of interparticle contacts. This leads to enhanced bulk flow in hoppers and chutes [10,11].

On the other hand, vibrations at high frequency and low amplitude lead to slow (logarithmic) decay of the pore space as a function of time [5]. Efficient vibrocompaction of dry and wet granular materials is a crucial issue in numerous applications, such as the casting of fresh concrete. The tamping operation on railway ballast is another example where the vibrations of tamping bars are used to restore the initial geometry of the track distorted as a result of ballast settlement [12–14]. The maintenance cost becomes crucial with the increase of commercial speed.

We may distinguish two methods for inducing vibrational dynamics: (1) by imposed cyclic displacements of a wall or the container (shaking) and (2) by cyclic modulation of a confining stress. The first method has been used in most experiments on granular beds [15–20]. In this case, the control parameters are the amplitude a and the frequency ν of the vibrations corresponding to a maximal acceleration $a\omega^2$ where $\omega=2\pi\nu$. When a material is molded inside a closed box, the vibrations should rather be induced by varying a confining force, e.g., a force acting on a wall. Then, the amplitude of displacements is a function of the forcing frequency, and the level of particle accelerations depends on both the applied cyclic force and the reaction force of the packing. In any case, an efficient compaction process requires periods of release of the packing so that the grains can move with respect to their neighbors.

In this paper, we explore such a system where a harmonic force f is exerted on a vertical wall of a box, all other walls remaining immobile. The force f is varied between zero and a maximum value f_{max}. During a period, f is large enough to equilibrate the packing reaction force except for a short lapse of time when f declines to zero. Then, the packing can flow under the action of its own weight, pushing the retaining wall away. We are interested here in the evolution of the packing in the course of harmonic loading and its scaling with loading parameters (frequency, force maximum).

We used numerical simulations by the contact-dynamics approach as a discrete element method (DEM) in a two-dimensional geometry with a small number of particles [21,22]. Each simulation is repeated for several independent configurations and the results are analyzed in terms of ensemble-average behaviors. The particles are rigid and polygon-shaped. We focus on the displacements of the free retaining wall and the compaction of the packing. Most results presented below concern the short-time behavior where the solid fraction increases linearly with time. The frequency is varied from 1 to 60 Hz and its influence is analyzed by considering characteristic times involved in the loading and unloading intervals of time. We first introduce the numerical procedures. Then, we present the main findings concerning the passive and active dynamics, the evolution of the solid

*Electronic address: azema@lmgc.univ-montp2.fr

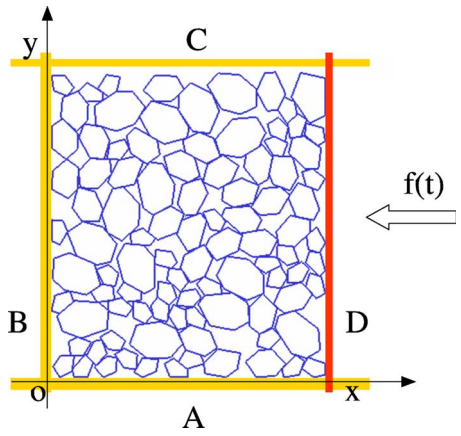

FIG. 1. (Color online) The geometry of the packing.

fraction, and scaling with the loading parameters.

II. NUMERICAL PROCEDURES

The simulations were carried out by means of the contact-dynamics (CD) method with irregular polygonal particles [21,22]. The CD method is based on implicit time integration of the equations of motion and a nonsmooth formulation of mutual exclusion and dry friction between particles. This method requires no elastic repulsive potential and no smoothing of the Coulomb friction law for the determination of forces. For this reason, the simulations can be performed with large time steps compared to molecular-dynamics simulations. We used LMGC90, which is a multipurpose software developed in our laboratory, capable of modeling a collection of deformable or undeformable particles of various shapes by different algorithms [23].

The samples are composed of irregular pentagons, hexagons, and heptagons of three different diameters: 50% of diameter d_{min}=2.5 cm, 34% of diameter 3.75 cm, 16% of diameter d_{max}=5 cm; see Fig. 1. The particles are initially placed on a square network in a rectangular box and compressed by a downward motion of the upper wall (wall *C* in Fig. 1) at zero gravity. Then, the gravity is set to g and the upper wall is raised 1 cm and fixed. The right wall (wall *D* in Fig. 1) is allowed to move horizontally (x direction) and subjected to a driving force:

$$f(t) = \frac{(f_{max} + f_{min})}{2} - \frac{(f_{max} - f_{min})}{2} \sin \omega t, \qquad (1)$$

where f_{max} and f_{min} are the largest and lowest compressive (positive) forces acting on the wall.

If f_{min} is above the (gravitational) force exerted by the grains on the free wall, f will be large enough to prevent the wall from backward motion during the whole cycle. In other words, the granular material is in a "passive state" in the sense of Rankine's states and the major principal-stress direction is horizontal [24]. In this limit, no extension will occur following the initial contraction. On the other hand, if f_{max} is below the force exerted by the grains, f will never be large enough to prevent the extension of the packing. This

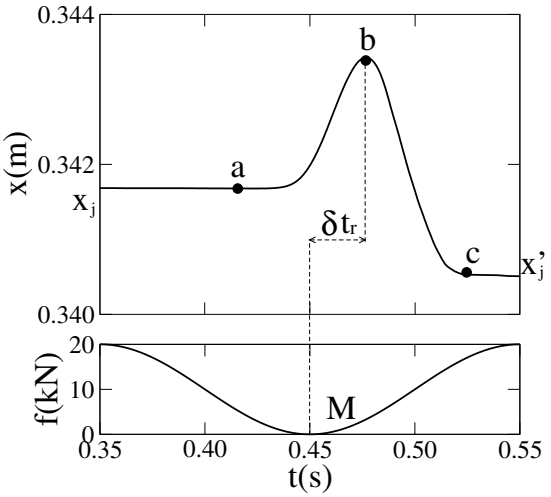

FIG. 3. A zoom on a single period (see Fig. 2).

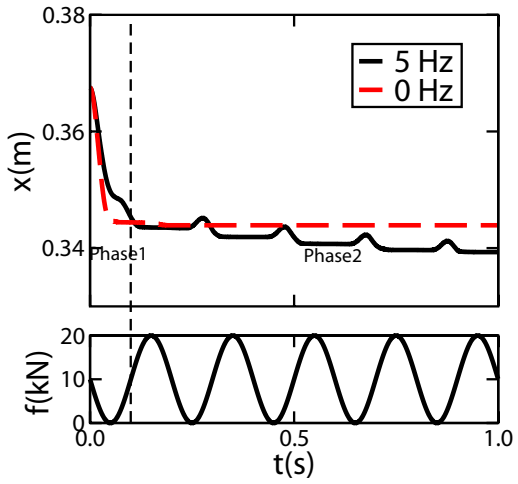

FIG. 2. (Color online) The evolution of the displacement x of the free wall (up) in response to harmonic loading (down).

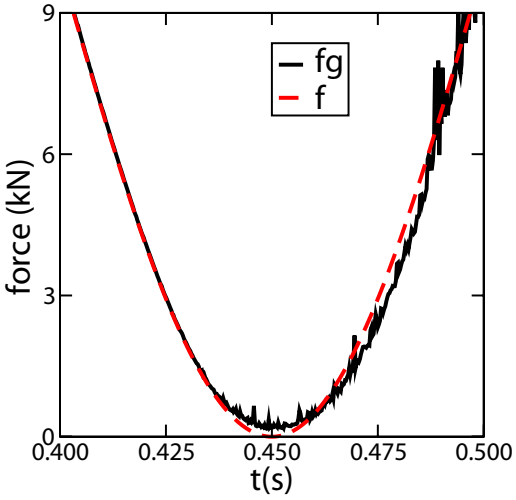

FIG. 4. (Color online) The force f_g exerted by the grains and the driving force f on the free wall as a function of time t.

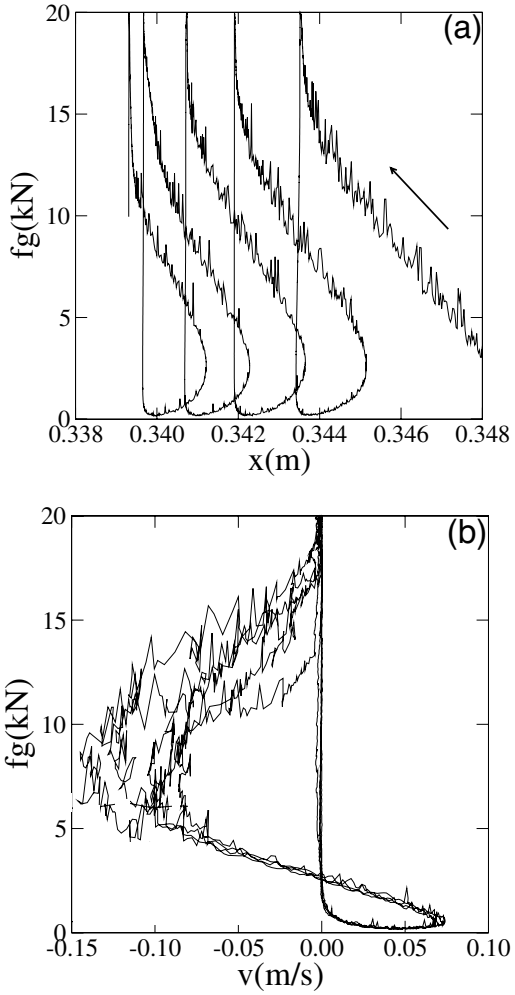

FIG. 5. Force f_g exerted by the grains on the free wall as a function of displacement x (a) and the velocity v (b).

corresponds to the "active state" where the major principal-stress direction remains vertical. In all other cases, both contraction and extension occur during each period, and the displacement Δx of the free wall will be controlled by f_{min}. In the simulations reported below, we set $f_{min}=0$. This ensures the largest possible displacement of the wall in the active state. We used four different values of f_{max} ranging from 5×10^3 N to 2×10^4 N.

The simulations were carried out with $N_p=95$ grains in the box and each simulation was repeated with seven independent grain configurations. The mean behavior for each set of parameters is obtained by ensemble averaging over seven independent data sets. Larger samples can be simulated, but that requires much more computational effort for a parametric study over many cycles. We checked that the dynamics and the scaling behavior remain basically the same in samples containing four times more particles than the samples studied in this paper. This point will be briefly illustrated in Sec. VI.

Thus, our system represents a rather thin granular layer. The coefficient of friction between the grains and with the horizontal walls was fixed to 0.4, but it was 0 at the vertical walls. With a time step equal to 2.5×10^{-4} s, we could perform high-quality simulations in which the largest cumulative error on grain positions was below 1%.

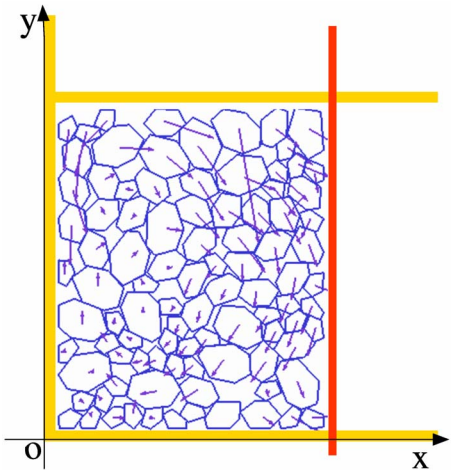

FIG. 6. (Color online) Particle displacements over one period.

III. ACTIVE AND PASSIVE DYNAMICS

We first consider the motion $x(t)$ of the free wall (wall D in Fig. 1), which reflects the dynamics of the grains in the cell in response to harmonic forcing. Figure 2 shows $x(t)$ (averaged over seven independent simulations) for frequency $\nu=5$ Hz over a time interval $\Delta t=1$ s. We distinguish a fast initial contraction ($t<0.1$ s) followed by slow contraction (decreasing x) over four periods. The initial contraction is a consequence of the gap left between the free surface of the packing and the upper wall. This initial volume change is almost independent of frequency. The subsequent periodic motion of the wall takes place around this confined state and will be the focus of this paper.

A zoom on a single period is shown in Fig. 3. The period begins at the jamming position $x=x_j$ corresponding to the jamming position reached in the preceding period. The motion of the wall begins (point a in Fig. 3) only when the applied force f declines near to its minimum $f_{min}=0$. The maximum displacement Δx_{max} occurs at a later time δt_r (point b). From a to b, the force exerted by the packing on the free wall is above the applied force, so that the wall moves backward (extension). In this phase, the packing is in an active state. The inverse situation prevails from b to c where the grains are pushed towards the box (contraction). Then, the packing is in a passive state. The new jamming position x_j' is below the jamming position x_j reached at the end of the preceding period. The difference x_j-x_j' represents the net compaction of the packing over one period. For a given frequency ν, the phase difference δt_r is the same for all periods. The displacement amplitude Δx_{max} is a function of f_{max} and ν, as we shall see below.

The motion of the free wall is governed by the equation of dynamics,

$$f-f_g=m_w\ddot{x}, \tag{2}$$

where f_g is the horizontal force exerted by the packing on the wall and m_w is the mass of the wall (Fig. 1). Figure 4 dis-

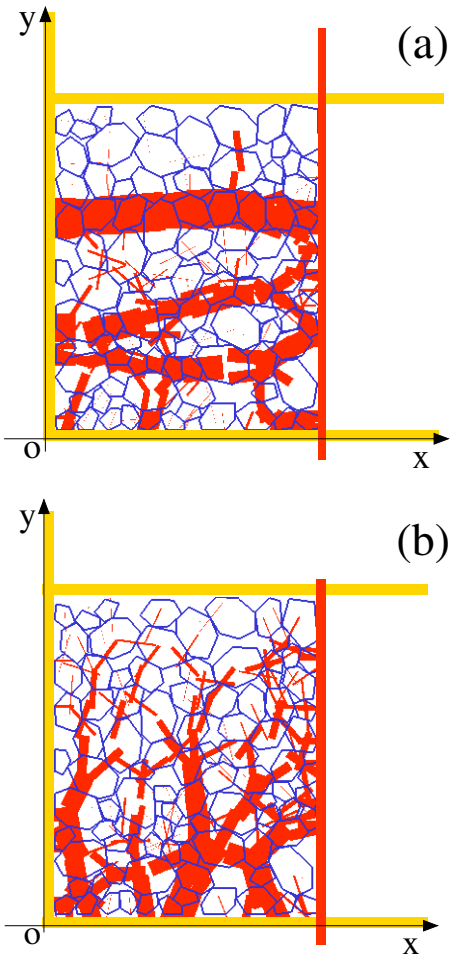

FIG. 7. (Color online) Normal forces in the passive (a) and active (b) states. Line thickness is proportional to the force.

plays f_g as the function of time for $f_{max}=2\times10^4$ N. We see that f_g follows closely the variations of f. In particular, in the jammed state we have $f=f_g$ so that $\ddot{x}=0$ in this state. This means that, in its most general form, f_g is a function of f.

Figure 5(a) shows f_g vs x over four periods. In the active phase, f_g grows slightly with x. In the passive phase, it grows faster and almost linearly as x decreases. The vertical line corresponds to the jammed state where f_g decreases with f at $x=x_j$. We also clearly observe in Fig. 5(a) two transients: (1) unjamming and the onset of the active state and (2) jamming from the passive state. It is remarkable that, although x_j decreases at the end of each period, the dynamics remains self-similar up to a translation along displacement coordinates.

Figure 5(b) displays f_g as a function of the velocity $v \equiv \dot{x}$. We again observe the passive ($v<0$) and active ($v>0$) states together with the jamming and unjamming transients before and after the jammed state ($v=0$ and $x=x_j$). The data from all periods follow the same variations except for the jamming transient where a slight decrease of the maximum negative velocity v_{max} can be noticed in each period.

Although we focus here on the average dynamics of the packing, i.e., the displacements of the free wall, it is important to note that the grain-velocity field is not a simple oscillation around an average position. The grains undergo a clockwise convective motion in the cell as shown in Fig. 6. On the other hand, the contact forces evolve between a fully jammed state, where nearly horizontal-force chains dominate [Fig. 7(a)], and the active state, where nearly vertical gravity-induced chains can be observed [Fig. 7(b)].

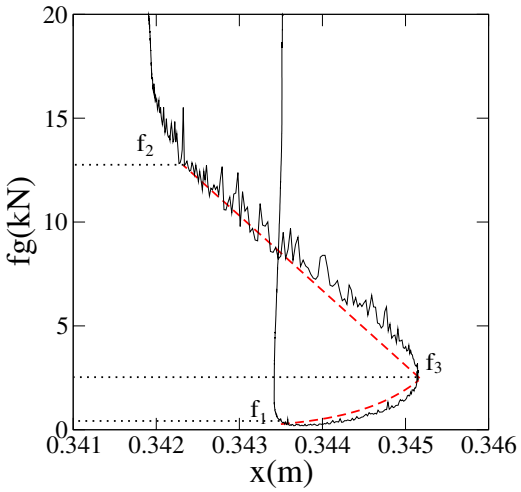

FIG. 8. (Color online) Variation of the packing reaction force f_g with displacement x over one period (full line) and an approximate fitting form (dashed line).

IV. SIMPLE MODEL

To predict the motion of the free wall from Eq. (2), we need to express the force f_g as a function of x and v. It is obvious that in the jammed state at $x=x_j$, the force f_g is a reaction force balancing exactly the driving force f, so that $v=0$. On the other hand, the inertia effects are small compared to static forces. To show this, we may use a dimensionless number I defined by [25]:

$$I = \dot{\varepsilon}\sqrt{\frac{m}{p}}, \tag{3}$$

where $\dot{\varepsilon}=\dot{x}/x$ is the deformation rate, m is the total mass of particles, and p is the average pressure. We find that, even for our largest frequencies, we have $I<0.02$. This implies that f_g should not depend crucially on v. Let us note that the plot of f_g vs v in Fig. 5(b) does not represent the *explicit* dependence of f_g on v; it is a consequence of the equation of dynamics and, as we shall see below, it can be reproduced by assuming that f_g is independent of v.

We now introduce a simple model in which the expression of f_g as a function of x is extracted from the numerical data plotted in Fig. 5(a). As shown in Fig. 8, two distinct fitting forms should be considered for the active and passive states. Ignoring the jamming and unjamming short transients, an exponential form provides a nice fit for the active branch, whereas a linear fit is a fairly good approximation in the passive state. Formally, we have

$$f_g = \begin{cases} \alpha + \beta e^{k(x-x_j)}, & \text{active} \\ \alpha' + \beta'\{1 + k'(x-x_j)\}, & \text{passive}, \end{cases} \tag{4}$$

with

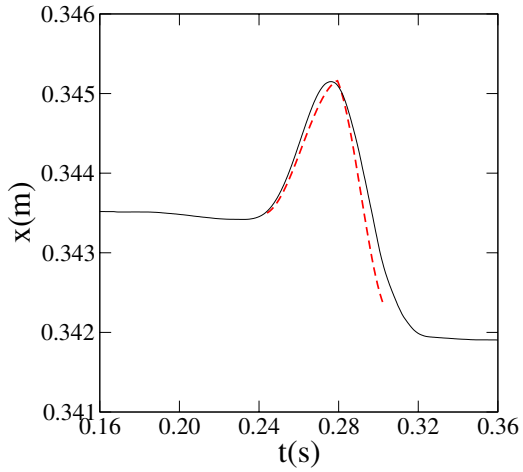

FIG. 9. (Color online) Displacement x of the free wall as a function of time (full line) and analytical fit from the phenomenological model (dashed line).

$$\alpha = (f_3 - f_1 e^{k\Delta x_{max}})/(1 - e^{k\Delta x_{max}}),$$

$$\beta = (f_1 - f_3)/(1 - e^{k\Delta x_{max}}),$$

$$\alpha' = [f_2(1 + k'\Delta x_{max}) - f_3]/(k'\Delta x_{max}),$$

$$\beta' = (f_3 - f_2)/(k'\Delta x_{max}). \quad (5)$$

The constant forces f_1, f_2, and f_3 correspond to the values of f_g at the unjamming transient, the jamming transient, and the point of transition from active to passive states, respectively (see Fig. 8). Clearly, because of the action of gravity and the jamming transition, we have $f_1 > f_{min}$ and $f_2 < f_{max}$.

We substitute the expression (4) in Eq. (2) and we solve for x. An analytical solution can be obtained for the passive linear part. An approximate solution can be given also for the active part by expending the exponential function to leading order. Figure 9 shows the evolution of the position x for one period together with the solution of the model.

The parameters k and k' are adjusted in order to get the best fit for the plot. The continuity of the fit at a transition between passive and active states is ensured by the very choice of the coefficients according to Eq. (5). Although we did not take into account the transients, the analytical plot correctly fits the data.

Figure 10 displays f_g vs v for one period, together with the analytical fit obtained as a solution to Eq. (2) with the expression (4) of f_g as a function of x. Again, excluding jamming and unjamming transients, the analytical solution provides a fairly good approximation for the simulation data although the largest contraction velocity is underestimated in the passive state.

The model parameters k and k' remain nearly the same over all periods. This means that the dynamics at short times ($\Delta t < 1$ s) is weakly dependent on the solid fraction. The parameters k and k' change, however, with loading parameters (ν, f_{max}, etc.) unless the displacements and the forces f_1, f_2, and f_3 are scaled with these parameters.

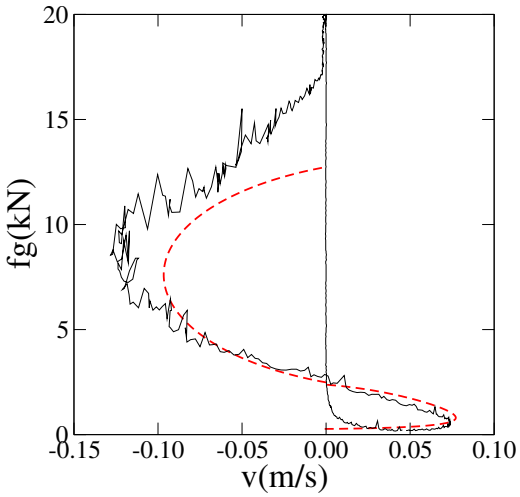

FIG. 10. (Color online) Force f_g exerted by the grains on the free wall vs velocity v over one period (full line) and analytical fit from the integration of the equation of dynamics using Eq. (4) (dashed line).

V. COMPACTION

In order to evaluate the solid fraction ρ, we consider a control volume enclosing a portion of the packing inside the simulation cell. This volume does not include the initial gap between the top of the packing and the upper wall. The initial value of the solid fraction is 0.75 and, since the grains are angular-shaped, its variations $\Delta\rho$ from the initial state are large.

Figure 11 shows the evolution of $\Delta\rho$ for several periods. We observe an initial compaction of 3% occurring in 0.1 s. The subsequent evolution of the solid fraction takes place in a more compact state with a small increase in each period.

We use $\rho_0 = 0.77$ at the end of the first period as the reference value for solid fraction. The relative compaction of the packing is given by $\Delta\rho/\rho_0$. The compaction rate $\dot{\eta}$ over several periods and for a total time interval Δt is

$$\dot{\eta} \equiv \frac{1}{\rho_0}\frac{\Delta\rho}{\Delta t}. \quad (6)$$

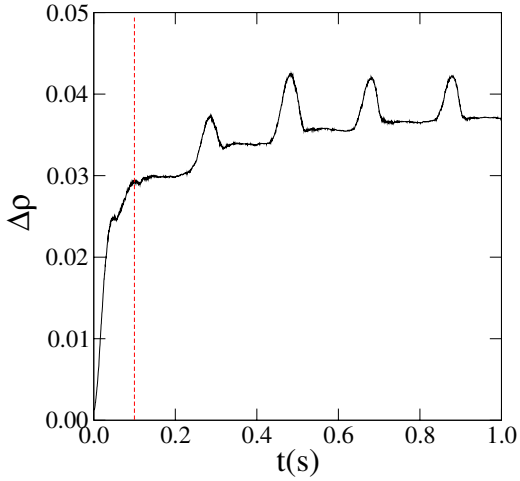

FIG. 11. (Color online) Evolution of the solid fraction $\Delta\rho$ from the initial state as a function of time over several periods.

Figure 12 shows the jamming position x_j as a function of time for different frequencies for $\Delta t < 1$ s. At such short times, it can be assumed, with a good approximation, that the solid fraction declines linearly in time. Generally, the behavior slows down logarithmically at longer times [16]. This means that at short times, in which we are interested in this paper, the compaction rate is nearly constant, and we have

$$\dot{\eta} = \frac{\Delta\rho_1}{\rho_0}\nu, \tag{7}$$

where $\Delta\rho_1$ is the compaction per period. For $\nu = 5$ Hz and $f_{max} = 2 \times 10^4$ N, we have $\dot{\eta} \simeq 0.009$ s^{-1}.

Interestingly, compaction occurs in the active state, i.e., during the extension of the packing, and not during contraction. This is shown in Fig. 13, where the variation $\Delta\rho$ of the solid fraction is plotted as a function of x. The solid fraction increases during extension (increasing x) and decreases during contraction (decreasing x).

Compaction upon the reversal of the direction of shearing is a well-known property of granular media [26]. Low-amplitude cyclic shearing leads to cumulative compaction of a granular material. At larger amplitudes, the compaction is followed by decompaction (dilation) and no net compaction can be observed over a full cycle. The situation is slightly different in our system in the presence of a jammed state. Compaction is a consequence of unjamming and it is pursued during the whole active state. Decompaction takes place in the passive state, but it is cut short by fast jamming. The outcome of a full cycle is thus a net compaction of the packing.

VI. SCALING WITH LOADING PARAMETERS

In the last three sections, we analyzed the vibrational dynamics and compaction for a single frequency $\nu = 5$ Hz. Similar simulations were performed for several frequencies ranging from 1 to 60 Hz. Up to a change in time and length scales, all simulations yield similar results both for dynamics

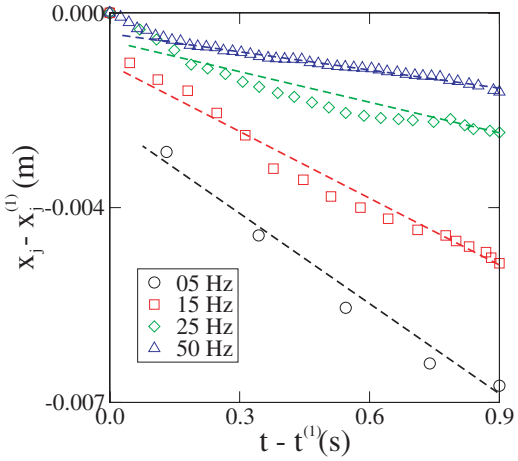

FIG. 12. (Color online) Evolution of the jamming position x_j from the position $x^{(1)}$ reached at $t = t^{(1)} = 0.1$ s for four different frequencies.

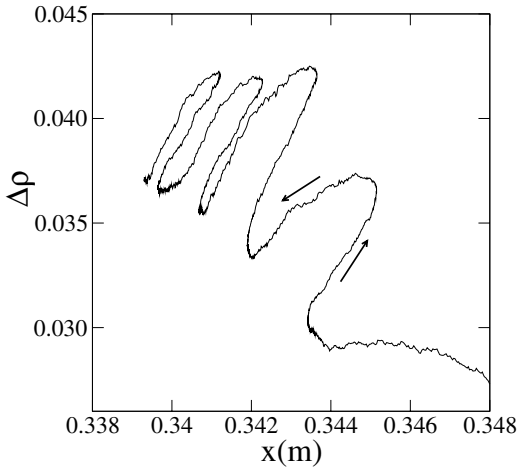

FIG. 13. Variation $\Delta\rho$ of the solid fraction from the initial state as a function of the displacement x of the free wall.

and compaction independently of the applied frequency. This can be seen, for example, in Fig. 14(a), where the phase-space trajectory is shown for $\nu = 5$ Hz and $\nu = 10$ Hz. Figure 14(b) shows that the data from both simulations collapse nicely on the same curve by simply scaling the displacements Δx by ν^{-2} and the velocities v by ν^{-1}.

This scaling is suggested by a dimensional analysis of the average dynamics of the packing. The frequency ν sets the time scale $\tau = \nu^{-1}$. Force scales are set by the largest driving force f_{max} in the passive state and the grain weights mg as well as the smallest driving force f_{min} in the active state. Hence, dimensionally, for fixed values of mg, f_{min}, and f_{max}, all displacements are expected to scale with ν^{-2} and all velocities with ν^{-1}. To directly check this scaling, in Fig. 15 we have plotted the maximum displacement Δx_{max} in the active state and the maximum velocity v_{max} in the passive state as a function of ν. The corresponding fits by ν^{-2} and ν^{-1} are excellent.

The influence of loading-force parameters mg, f_{min}, and f_{max} should be analyzed separately for each regime. In the passive state, f_{max} is the dominant force and it is exactly balanced by f_g in the jamming transition. On the other hand, in the active state, mg is the dominant force as f remains small compared to mg in this state. The maximum displacement Δx_{max} at the transition from active to passive state is determined in a subtle way by both f_{max} and mg. If gravity were the only driving force in the active state, Δx_{max} would simply scale with $g\nu^{-2}$ independently of f_{max}. However, our data show that Δx_{max} varies as f_{max}^{-1} (see Fig. 16).

A plausible dimensional interpretation is to assume that Δx_{max} is controlled by the ratio mg/f_{max} representing the relative importance of the gravitational-to-loading forces. On the other hand, the mass ratio m_w/m controls the inertia, and thus the maximum displacement of the wall governed by Eq. (2). Varying systematically m_w, we found that Δx_{max} varies as $m/(m+m_w)$. Thus, we propose the following expression for the scaling with loading forces:

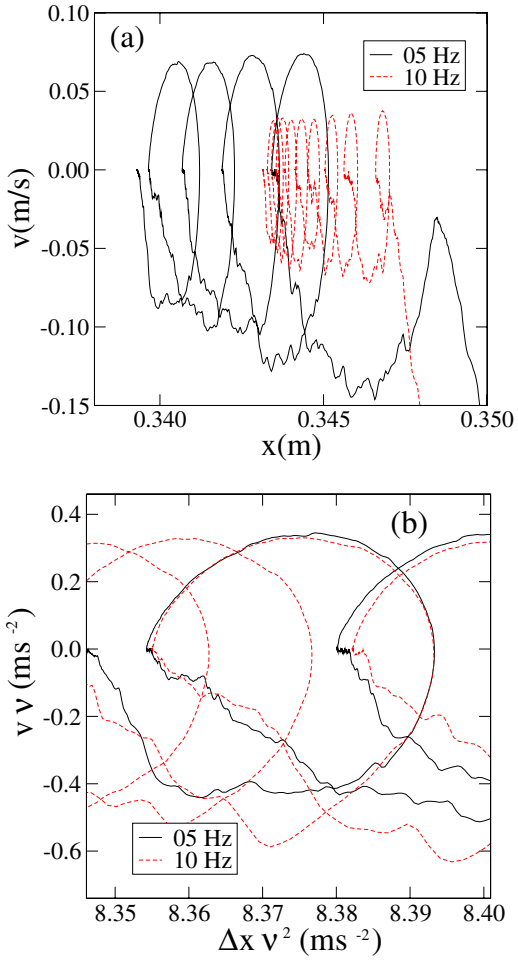

FIG. 14. (Color online) Phase-space trajectories for two frequencies without scaling (a) and with scaling (b) of the displacements and velocities.

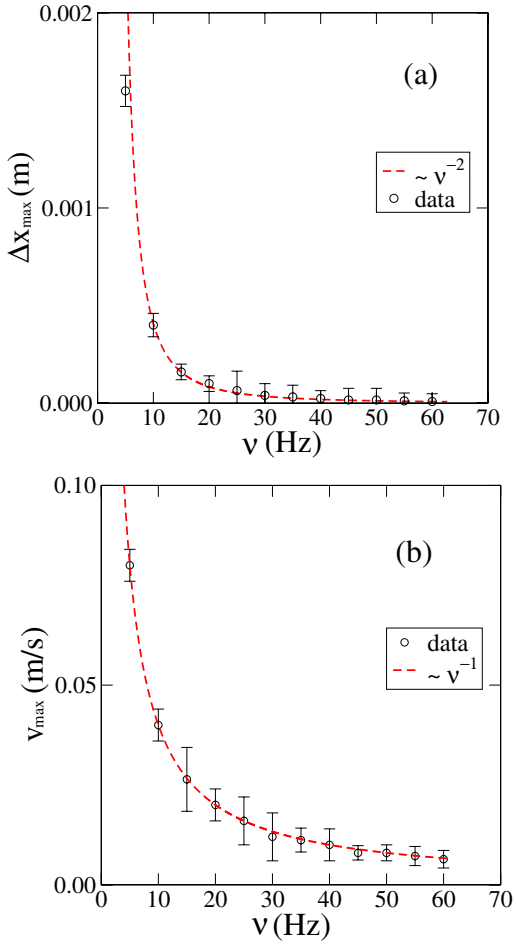

FIG. 15. (Color online) Maximum displacement Δx_{max} (a) and the maximum velocity v_{max} (b) as a function of the frequency ν.

$$\Delta x_{max} = C\left(\frac{m}{m+m_w}\right)\left(\frac{mg}{f_{max}}\right)\left(\frac{g}{\nu^2}\right), \tag{8}$$

where C is a dimensionless prefactor. This equation includes the correct scaling of Δx_{max} with the frequency ν [Fig. 15(a)], with the force f_{max} (Fig. 16), and with the mass m_w of the wall.

Interestingly, Eq. (8) predicts that Δx_{max} varies as g^2. This prediction is again in excellent agreement with our simulation data shown in Fig. 17 for four different values of g.

Equation (8) implies that the prefactor C is a material constant that remains independent of all our loading parameters and m_w. Figure 18 shows Δx_{max} as a function of $(mg)^2/[(m+m_w)(f_{max}\nu^2)]$ from different simulations with different values of ν, f_{max}, g, and m_w. The data are in excellent agreement with the scaling suggested by Eq. (8) with $C \simeq 0.05$. Figure 18 also contains a point representing a system of 400 particles. This point lies on the same plot with all other points, showing that the scaling behavior does not crucially depend on the system size although the jamming transition is basically controlled by the presence of the rigid walls in all cases.

The above scaling can be incorporated in the fitting form (4) expressing f_g as a function of $x-x_j$ and three forces f_1, f_2, and f_3 (see Fig. 8). In this fitting form, the displacements should be divided by Δx_{max}. We will not study here in detail the dependence of f_1, f_2, and f_3 with respect to loading force parameters mg, f_{min}, and f_{max}. Our simulations show that f_3 is independent of f_{max}, but it depends linearly on mg. Theoretically, this state corresponds to the limit-active state where the ratio of principal stresses is a function of the internal angle of friction [24]. On the other hand, the force f_2 simply scales as f_{max}, and f_1 depends both on f_{min} and mg. In our simulations, where $f_{min}=0$, the force f_1 is close to zero.

VII. COMPACTION RATES

Equation (7) suggests that the compaction rate $\dot{\eta}$ should vary linearly with the frequency ν if the total compaction per period $\Delta\rho_1$ is independent of ν. Figure 19 shows $\dot{\eta}$ as a function of ν. We see that only at low frequencies, $\dot{\eta}$ increases linearly with ν. At larger frequencies, beyond a characteristic frequency ν_c, $\dot{\eta}$ declines with ν. The largest compaction rate $\dot{\eta}_{max}$ occurs for $\nu=\nu_c$. This implies that, according to Eq. (7), $\Delta\rho_1$ is indeed independent of ν for $\nu < \nu_c$. The characteristic time $\tau_c \equiv \nu_c^{-1}$ can be interpreted as

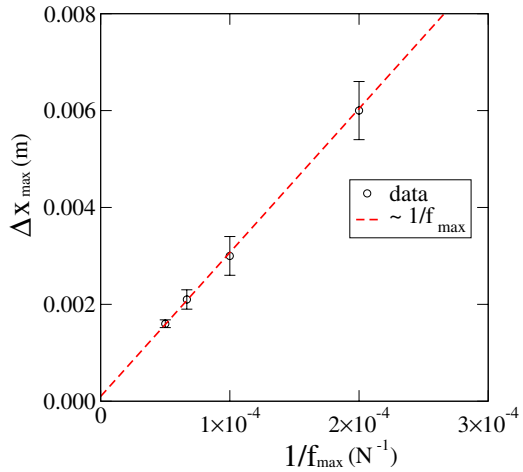

FIG. 16. (Color online) Scaling of the maximum displacement Δx_{max} with the force amplitude f_{max}.

the minimum time lapse required for the relaxation of the packing. In fact, in the active state, the packing needs a finite rearrangement time τ_c to achieve a higher level of solid fraction. As long as the period $\tau=\nu^{-1}$ is longer than the relaxation time τ_c, the packing has enough time to relax fully to a more compact state. Then, the compaction $\Delta\rho_1$ has its maximum value $\Delta\rho_{max}$. But, if the period τ is below τ_c, the relaxation will be incomplete so that $\Delta\rho_1 < \Delta\rho_{max}$.

Since the volume change ΔV is proportional to Δx, $\Delta\rho_1$ follows the same scaling with the frequency as the displacement of the retaining wall, i.e., $\Delta\rho_1 \propto \Delta\rho_{max}\nu^{-2}$. Hence, from Eq. (7) and imposing the continuity at $\nu=\nu_c$, we get

$$\dot{\eta} = \begin{cases} \dfrac{\Delta\rho_{max}}{\rho_0}\nu, & \nu < \nu_c \\ \dfrac{\Delta\rho_{max}}{\rho_0}\nu_c^2\nu^{-1}, & \nu > \nu_c. \end{cases} \tag{9}$$

This form (labeled 1) is plotted in Fig. 19 together with the data points. It is remarkable that, although ν_c is the only

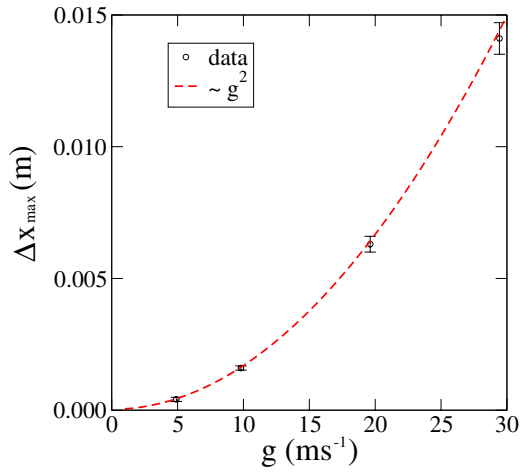

FIG. 17. (Color online) Scaling of the maximum displacement Δx_{max} with gravity g.

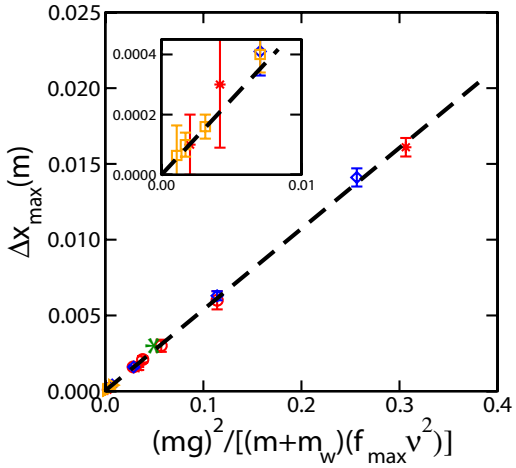

FIG. 18. (Color online) Scaling of the maximum displacement Δx_{max} with loading parameters from simulations with different values of the frequency ν (squares), the force amplitude f_{max} (circles), and the gravity g (diamonds) for the mass of the wall m_w (star) and for 400 particles (*). The inset shows the plot near the origin.

fitting parameter, the compaction rate $\dot{\eta}$ is well adjusted by Eq. (9). The prefactor $\Delta\rho_{max}/\rho_0$ is $\simeq 1.5\times10^{-3}$, corresponding to $\Delta\rho_{max} \simeq 1.1\times10^{-3}$.

The arguments behind the proposed form (9) imply a sharp transition at $\nu=\nu_c$. This is rather plausible in view of the numerical data shown in Fig. 19. Nevertheless, it is convenient to construct a single expression containing the correct behavior both at low and high frequencies. The following fitting form provides a good approximation as shown also in Fig. 19 (fitting form 2):

$$\dot{\eta} = \frac{\Delta\rho_{max}}{\rho_0}\frac{1+e^{-(\nu/\nu_c-1)^2}}{1+\left(\dfrac{\nu}{\nu_c}\right)^2}\nu. \tag{10}$$

We have $\nu_c \simeq 6$ Hz corresponding to a characteristic time $\tau_c = 0.17$ s. This time interval is long compared to single-grain dynamics under gravity. For instance, the time required for a small-sized grain in our samples to fall down a distance equal to its diameter is about 0.002 s. Several observations show that collective rearrangements in granular media are often a slow process [27]. Let us finally recall that our findings concern the short-time behavior ($\Delta t < 1$ s). At longer times, $\dot{\eta}$ declines with time, but the scaling with frequency according to Eq. (9) is expected to hold at each instant of evolution of the packing.

VIII. CONCLUSION

In this paper, we analyzed the short-time behavior of a constrained granular system subjected to vibrational dynamics. The vibrations are induced by harmonic variation of the force exerted on a free retaining wall between zero and a maximum force. The system as a whole has a single degree of freedom represented by the horizontal position of the free wall. This system involves a jammed state separating passive (loading) and active (unloading) states. The contact dynam-

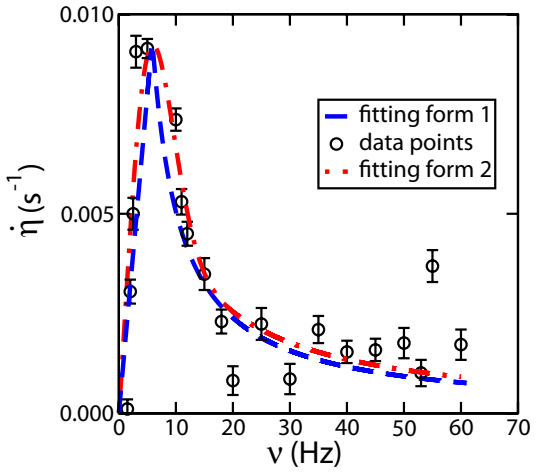

FIG. 19. (Color online) The compaction rate $\dot{\eta}$ as a function of the frequency (circles) fitted by two different functions (see the text.)

ics simulations were conducted with a rather small number of polygonal grains allowing for a systematic study of the dynamics and compaction of the material by varying the frequency and averaging over several configurations each time. By construction, our system is devoid of elastic elements and, hence, the behavior is fully governed by collective grain rearrangements.

In the loading phase, the reaction force (exerted by the grains on the free wall) rises almost linearly with the displacement of the free wall, but it increases considerably at the end of this phase in transition to the jammed state. This force enhancement features the jamming transition compared to the rest of the passive state. The reaction force decreases then in the jammed state, thus balancing exactly the driving force, until the latter is low enough for the grains to push the free wall away under the action of their own weights. This unjamming process occurs smoothly and the reaction force increases only slightly but exponentially during the unloading phase. We showed that a rough expression of the reaction force as a function of the displacement of the free wall with respect to the jamming position provides a good prediction of the dynamics except at the jamming and unjamming transients.

We used dimensional analysis to scale the dynamics with the frequency ν of oscillations. It was shown that the data for frequencies ranging from 1 to 60 Hz collapse by scaling the displacements by the inverse square of frequency. On the other hand, we studied both numerically and dimensionally the scaling with loading parameters mg and f_{max} as well as with the mass m_w of the free wall.

We also investigated the oscillatory compaction of our numerical samples. A small compaction occurs during unloading, i.e., during the extension of the sample, followed by a smaller decompaction during loading. The compaction rate is nearly constant for short times. It was shown that the compaction rate increases linearly with frequency up to a characteristic frequency and then it declines nearly in inverse proportion to frequency. The characteristic frequency was interpreted in terms of the time required for the relaxation of a packing in each period to a more compact state by collective grain rearrangements under the action of gravity. The decreasing compaction rate as a function of frequency beyond the characteristic frequency was explained by arguing that only a partial relaxation, inversely proportional to frequency, could occur at such frequencies.

A similar investigation is currently underway with polyhedral grains in three dimensions. Our preliminary results are consistent with those presented in this paper. In view of applications to a wider range of boundary conditions or diving modes, it is also important to consider in detail the characteristic time and the influence of various parameters pertaining to particle properties. Finally, long-time behavior and the slow evolution of the compaction rate may be studied in this framework though more numerical effort is necessary to reach significant results in this case.

ACKNOWLEDGMENTS

This work was funded by M. Valery from RFF (Réseau Ferré Français) and the Région Languedoc-Roussillon, who are gratefully acknowledged.

[1] J. B. Knight, C. G. Fandrich, C. N. Lau, H. M. Jaeger, and S. R. Nagel, Phys. Rev. E **51**, 3957 (1995).
[2] O. Sano, Phys. Rev. E **72**, 051302 2005).
[3] K. M. Aoki, T. Akiyama, Y. Maki, and T. Watanabe, Phys. Rev. E **54**, 874 (1996).
[4] K. Liffman, G. Metcalfe, and P. Cleary, Phys. Rev. Lett. **79**, 4574 (1997).
[5] J. B. Knight, H. M. Jaeger, and S. R. Nagel, Phys. Rev. Lett. **70**, 3728 (1993).
[6] K. M. Aoki and T. Akiyama, Phys. Rev. Lett. **77**, 4166 (1996).
[7] E. Clement, L. Vanel, J. Rajchenbach, and J. Duran, Phys. Rev. E **53**, 2972 (1996).
[8] H. M. Jaeger, S. R. Nagel, and R. P. Behringer, Rev. Mod. Phys. **68**, 1259 (1996).
[9] C. Brennen, S. Ghosh, and C. Wassgren, *Powders and Grains 93* (A. A. Balkema, Amsterdam, 1993), pp. 247–252.
[10] R. C. Weathers, M. L. Hunt, C. E. Brennen, A. T. Lee, and C. R. Wassgren, in "Effects of horizontal vibration on hopper flows of granular material," *Mechanics of Deformation and Flow of Particulate Materials*, edited by C. S. Chang, A. Misra, R. Y. Liang, and M. Babic (ASCE, New York, 1997) pp. 349–360.
[11] C. R. Wassgren, M. Hunt, P. Freese, J. Palamara, and C. Brennen, Phys. Fluids **14**, 3439 (2002).
[12] G. Saussine, Ph.D. thesis, Université Montpellier II, 2004 (unpublished).
[13] X. Oviedo, Ph.D. thesis, LCPC (unpublished).
[14] J. M. E. Markland, Geotechnique **31**, 3367 (1981).

[15] S. Luding, Phys. Rev. E **52**, 4442 (1995).
[16] E. Ben-Naim, J. B. Knight, and E. R. Nowak, J. Chem. Phys. **100**, 6778 (1996).
[17] E. Ben-Naim, J. B. Knight, E. R. Nowak, H. M. Jaeger, and S. R. Nagel, in *Proceedings of the 17th Annual CNLS Conference on Nonlinear in Waves in Physical Phenomena, 1997* (ASCE, New York, 1998), p. 104.
[18] M. L. Hunt, R. C. Weathers, A. T. Lee, and C. E. Brennen, Physica (Amsterdam) **11**, 68 (1999).
[19] A. Kudrolli, Rep. Prog. Phys. **67**, 209 (2004).
[20] C. Josserand, A. V. Tkachenko, D. M. Mueth, and H. M. Jaeger, Phys. Rev. Lett. **85**, 3632 (2000).
[21] M. Jean and J. J. Moreau, in *Proceedings of Contact Mechanics International Symposium* (Presses Polytechniques et Universitaires Romandes, Lausanne, Switzerland, 1992), pp. 31–48.
[22] J. Moreau, in *Novel Approaches in Civil Engineering*, edited by M. Frémond and F. Maceri, Lecture Notes in Applied and Computational Mechanics, No. 14 (Springer-Verlag, Berlin, 2004), pp. 1–46.
[23] F. Dubois and M. Jean, *Actes du Sixième Colloque National en Calcul des Structures* (CSMA-AFM-LMS, Olens, 2003), Vol. 1.
[24] R. M. Nedderman, *Statics and Kinematics of Granular Materials* (Cambridge University Press, Cambridge, 1992).
[25] GDR MiDi, Eur. Phys. J. E **14**, 341 (2004).
[26] J. Mitchell and K. Soga, *Fundamentals of Soil Behavior* (Wiley, New York, 2005).
[27] S. Deboeuf, O. Dauchot, L. Staron, A. Mangeney, and J.-P. Vilotte, Phys. Rev. E **72**, 051305 (2005).